

# Spin Dynamics, Critical Scattering and Magnetoelectric Coupling Mechanism of $Mn_4Nb_2O_9$

Guochu Deng,<sup>1,\*</sup> Gang Zhao,<sup>2</sup> Shuang Zhu,<sup>2</sup> Zhenjie Feng,<sup>2</sup> Wei Ren,<sup>2</sup> Shixun Cao,<sup>2,†</sup> Andrew Studer,<sup>1</sup> and Garry J McIntyre<sup>1</sup>

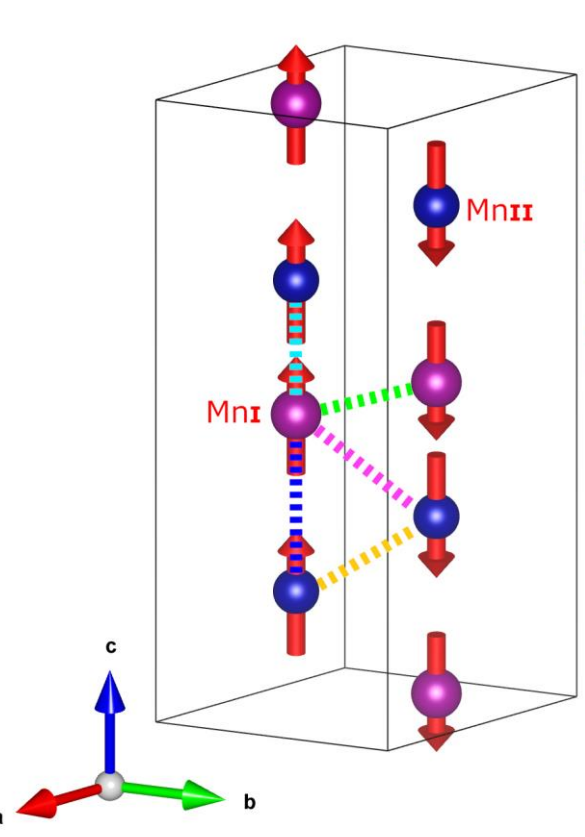
1. Australian Centre for Neutron Scattering, Australian Nuclear Science and Technology Organisation, New Illawarra Road, Lucas Heights NSW 2234, Australia  
2. Department of Physics, International Centre of Quantum and Molecular Structures and Materials Genome Institute, Shanghai University, Shangda Road 99, Shanghai 200444, People's Republic of China

## Abstract

The spin dynamics of  $Mn_4Nb_2O_9$  were studied by using inelastic neutron scattering. A spin-dynamic model is proposed to explain the observed spin-wave excitation spectrum. The model indicates that the exchange interactions along the chain direction are weakly ferromagnetic while the exchange interactions between the neighbor chains are strongly antiferromagnetic. Such a antiferromagnetic configuration in the hexagonal plane cause spin frustration with a spin gap of about 1.4 meV at the zone center. The  $Mn^{2+}$  ions in this material demonstrate a very weak easy-axis single-ion anisotropy. Critical scattering in the vicinity of  $T_N$  was studied. On the basis of the magnetic structure and spin-dynamic models, the weak magnetoelectric coupling effect in  $Mn_4Nb_2O_9$  is ascribed to the weak magnetostriction due to the subtle difference between  $Mn^{2+}$  ions on the  $Mn_I$  and  $Mn_{II}$  sites.

## Introduction

**Magnetoelectric** materials are materials which are able to actively respond to both external magnetic field and electric fields. They are highly interesting for applications in devices such as sensors or actuators. Therefore, they are extensively studied in recent years. It is extremely important to understand the mechanism of the magnetoelectric coupling in these materials because it helps to improve their magnetoelectric properties and provides guideline for improving their properties.



$Mn_4Nb_2O_9$ : Space group: R3c1;  $T_N$ : ~108K

Fig. 1 The schematics of the collinear antiferromagnetic structure of  $Mn_4Nb_2O_9$  showing the antiferromagnetic interactions ( $J_a$ ,  $J_b$  and  $J_c$ ) between neighboring  $Mn_I - Mn_{II}$  chains and the ferromagnetic intrachain interactions ( $J_d$  and  $J_e$ ) along the c axis. The blue and pink spheres indicate the  $Mn^{2+}$  ions on the  $Mn_I$  and  $Mn_{II}$  sites, respectively

## Spin-wave Excitation of $Mn_4Nb_2O_9$

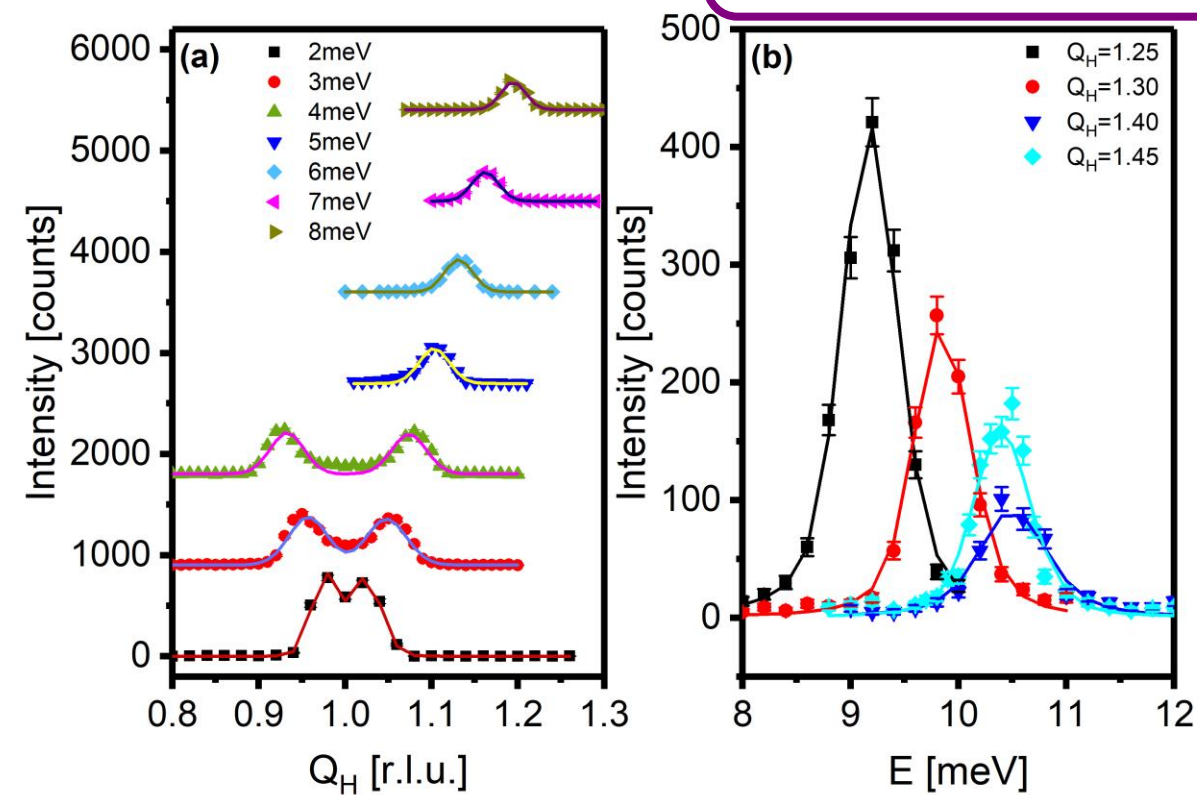


Fig. 2 (a) The constant-energy scans collected from 2 meV to 8 meV are plotted as symbols; the solid lines show the experimental data fitted by convoluting with the instrument resolution. (b) The constant-Q scans at different Q positions close to the zone boundary  $Q(1\ 0\ 1)$ .

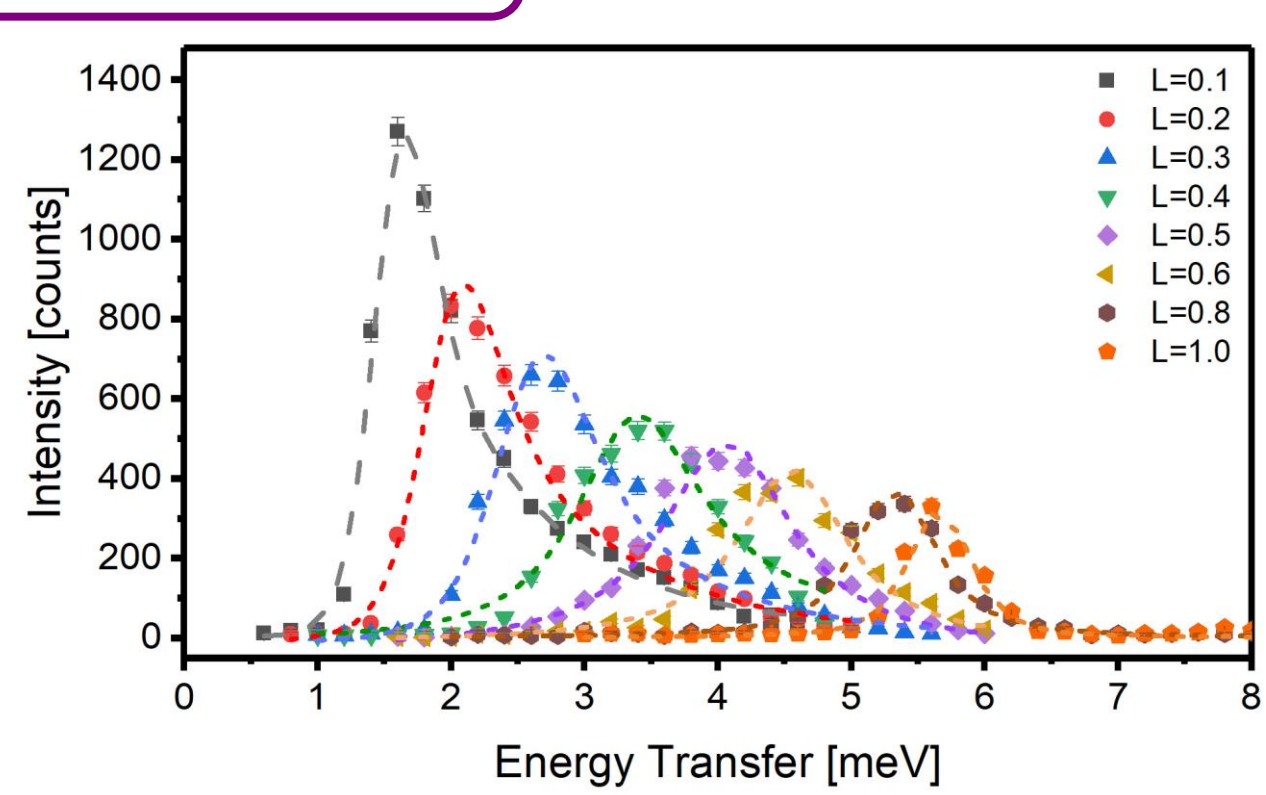


Fig. 3 (a) Energy scans conducted at a series of QL positions from the antiferromagnetic zone center (1 0 0) to the zone boundary (1 0 1). The excitation peak at the zone center show an energy gap of ~ 1.4meV.

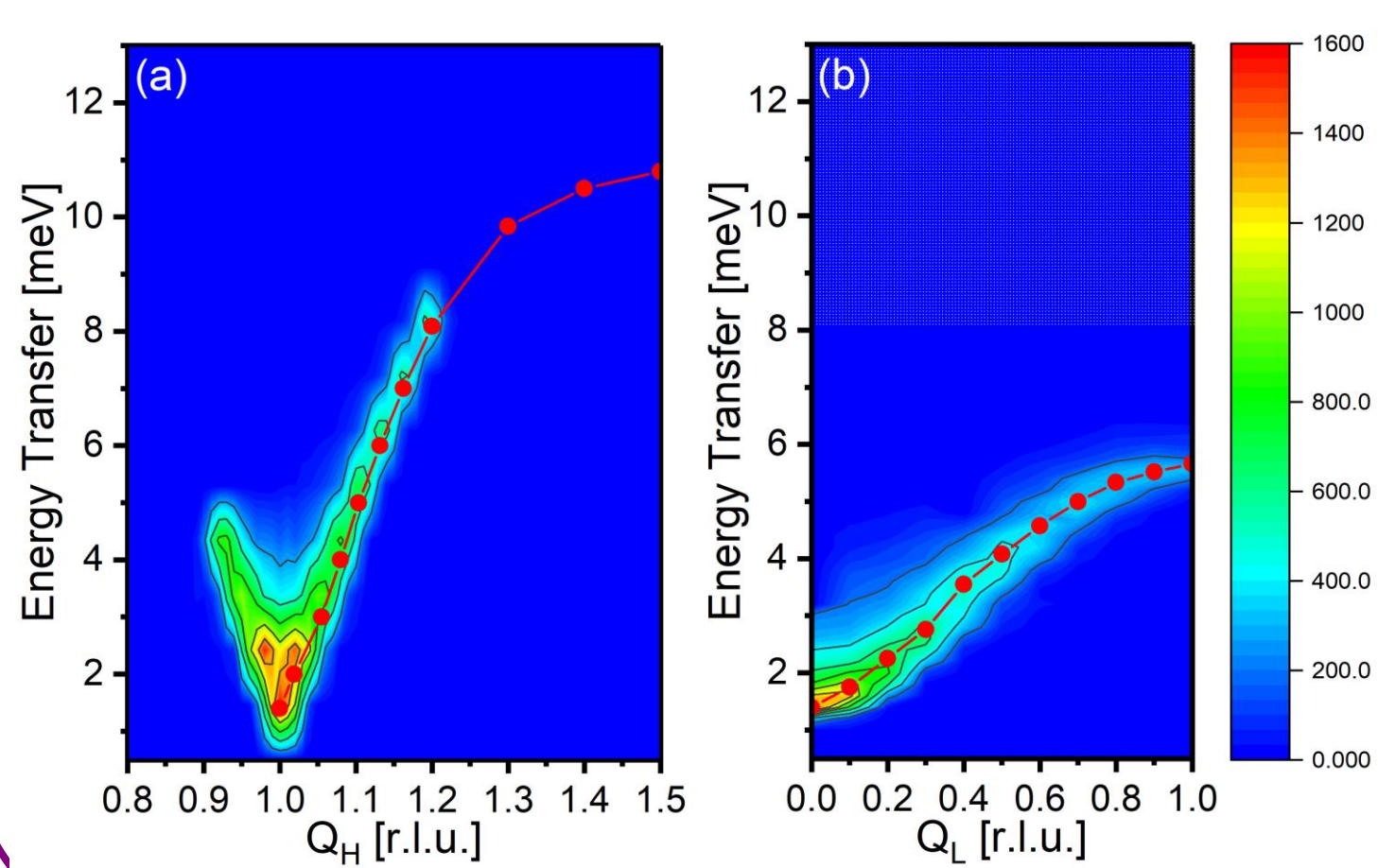


Fig.3 The false-color contour maps of the spin-wave dispersion measured from  $Mn_4Nb_2O_9$  along the (a)  $Q_H$  and (b)  $Q_L$  directions. The red dotted curves show the fitted peak positions from the experimental data. The contour map in (a) is constructed from the constant-energy scans while the contour map in (b) is constructed by the constant-Q scans. The dotted area in (b) is not scanned. The maps in (a) and (b) use the same energy scale for the convenience. The two maps are normalized to the same intensity level as well, as shown in the color bar on the right.

## Spin-wave Dynamic Model Fitting

$$H = J_d \sum_{i,j} \vec{S}_i^I \cdot \vec{S}_j^{II} + J_e \sum_{i,j} \vec{S}_i^I \cdot \vec{S}_j^{II} + J_a \sum_{i,j} \vec{S}_i^{II} \cdot \vec{S}_j^{II} + J_b \sum_{i,j} \vec{S}_i^I \cdot \vec{S}_j^I + J_c \sum_{i,j} \vec{S}_i^I \cdot \vec{S}_j^I + D \sum_{Mn_I} (\vec{S}_i^I)^2 + D \sum_{Mn_{II}} (\vec{S}_i^{II})^2$$

Where the exchange interactions  $J_a$ ,  $J_b$ ,  $J_c$ ,  $J_d$ ,  $J_e$  are described in the Fig. 1. Using the spin-wave calculation package SpinW,<sup>[1]</sup> fitting the experimental dispersion curve to the model above generates the parameters in the table below:

$J_a$ (meV)	$J_b$ (meV)	$J_c$ (meV)	$J_d$ (meV)	$J_e$ (meV)	D (meV)
1.34	2.83	0.178	-0.025	-0.026	-0.135

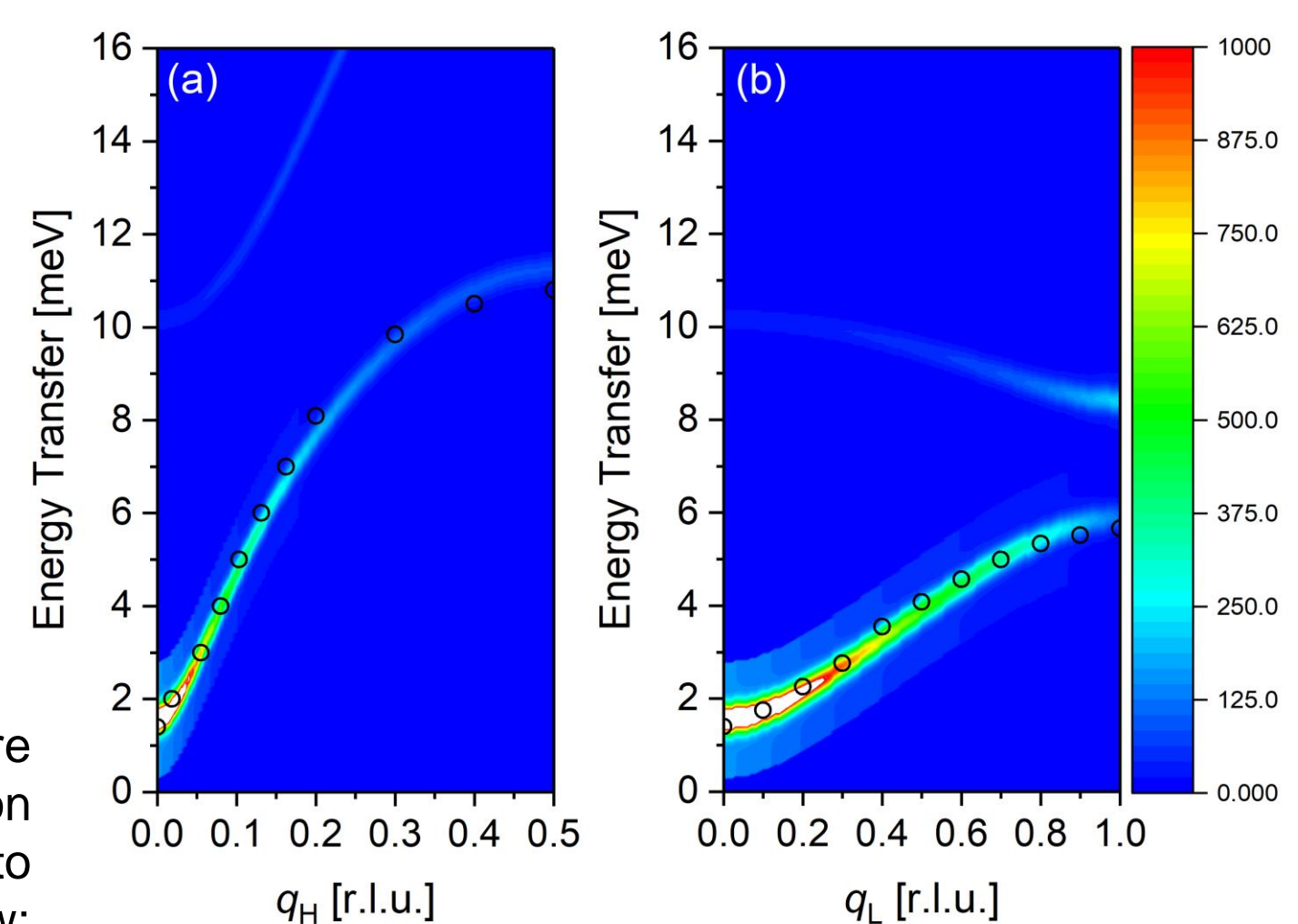


Fig. 4 The false-color contour maps of the spin-wave dispersion measured from  $Mn_4Nb_2O_9$  along the (a)  $Q_H$  and (b)  $Q_L$  directions. The circle symbol curves show the fitted peak positions from the experimental data. The contour map is from the simulated results from the dynamic models described on the left using the parameters in the table.

## Critical Scattering of $Mn_4Nb_2O_9$ Near $T_N$

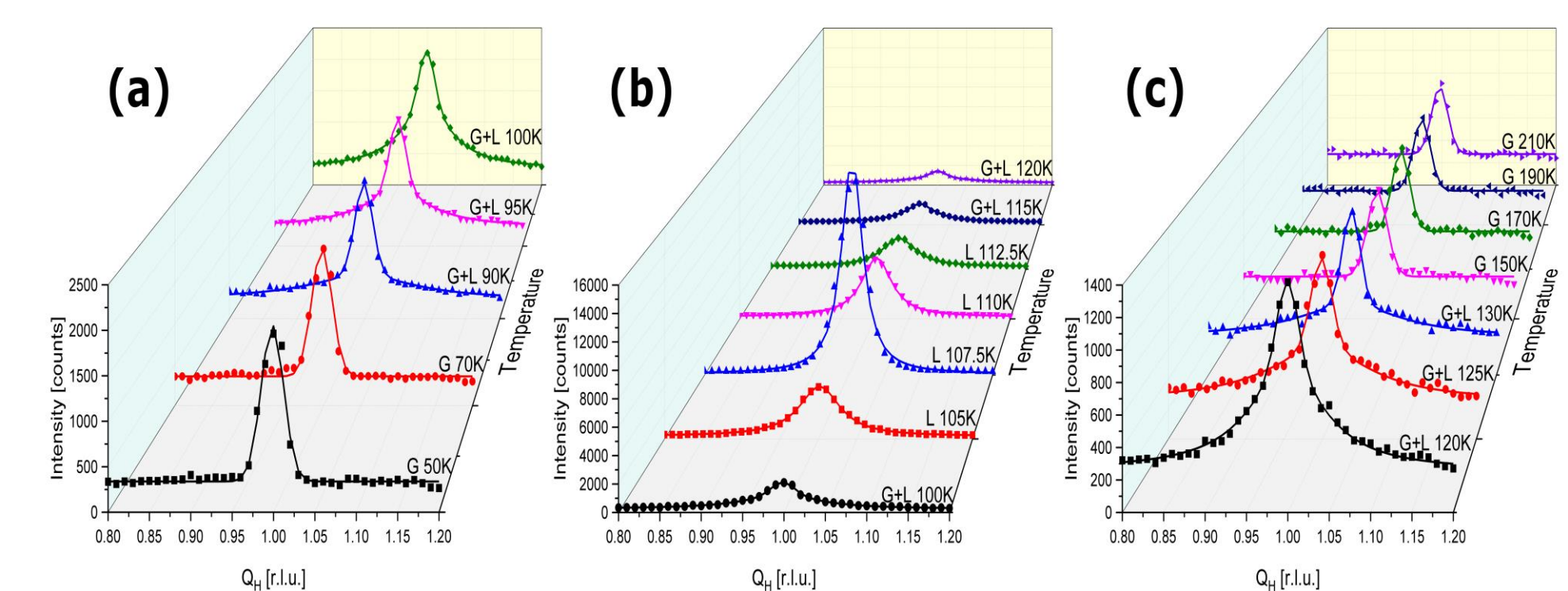
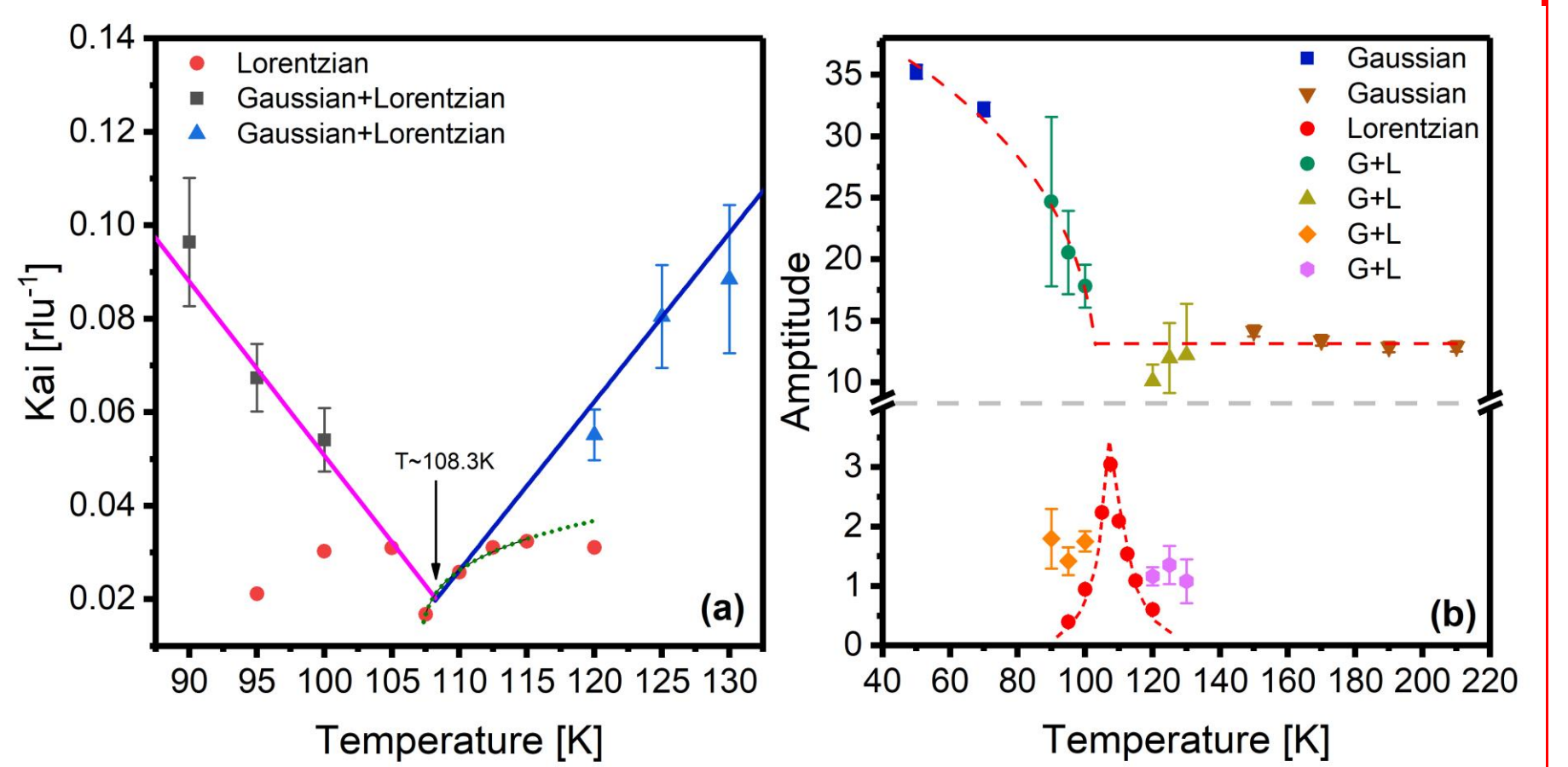


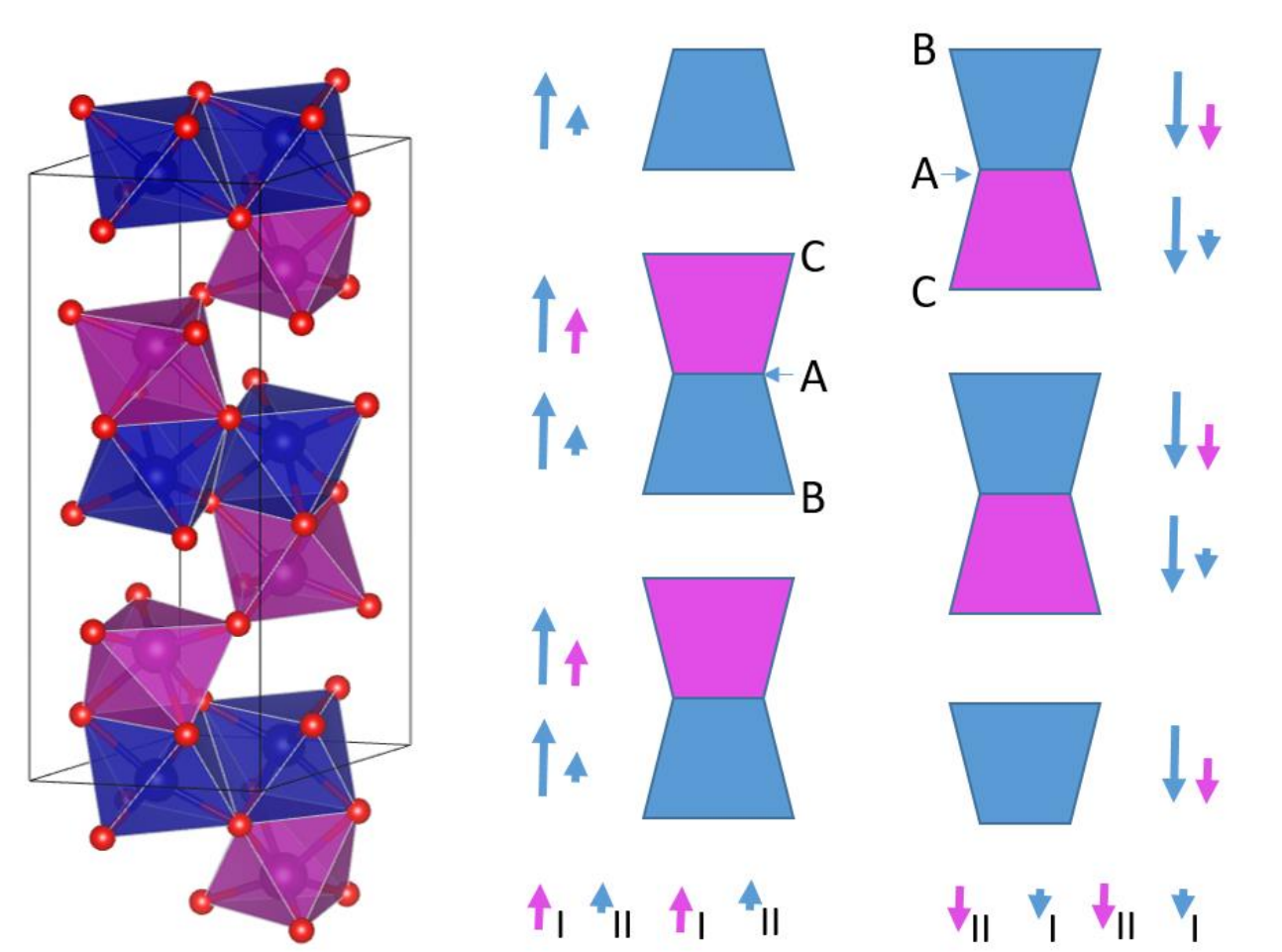
Fig. 5 The (1 0 1 0) Bragg peak of  $Mn_4Nb_2O_9$  measured (a) at 50K ~ 100K, (b) 100K ~ 120K, (c) 120K ~ 210K. "G" denotes that the curves were fitted to a Gaussian. "L" denotes that the curves were fitted to a Lorentzian. "G+L" denotes that the curves were fitted to a sum of a Gaussian and a Lorentzian. Diffuse scattering was observed in the temperature range near  $T_c$  of  $Mn_4Nb_2O_9$ .

Fig. 6 (a) The fitted  $\kappa$  values at different temperature from the data shown in Fig. 5. The black squares show the Gaussian + Lorentzian fit to the experimental data at low temperature. The blue triangles show the fitted values by using a function of Gaussian plus a Lorentzian. The red dot shows the fitted values by using a single Lorentzian function. The pink and blue lines are a guide to the eyes. The green dotted line is fitted to the power law mentioned in the text. (b) The fitted amplitude of the peaks at different temperatures with different fitting methods.



## Magnetoelectric Mechanism

FIG. 7. The  $Mn_I O_6$  (blue) and  $Mn_{II} O_6$  (purple) octahedra in the crystal structure of  $Mn_4Nb_2O_9$  (left). The schematics of the octahedra in the  $Mn_4Nb_2O_9$  lattice (right) in an external electric field. A, B, and C are the triangles described in the text. The long blue arrows indicate the magnetic moments in the  $Mn_4Nb_2O_9$  magnetic structure at zero field. The short arrows with two different colors indicate the changes of the magnetic moments when applying an electric field along the c axis. The arrows at the bottom shows all the changes of the magnetic moments on the two chains due to the applied electric field. If  $Mn_I O_6$  and  $Mn_{II} O_6$  are equivalent, then all the field-induced magnetization changes cancel out. However,  $Mn_I O_6$  and  $Mn_{II} O_6$  are non-equivalent according to the neutron powder diffraction, which causes the ME effect in this compound.<sup>[3]</sup>



## Comparison with $Co_4Nb_2O_9$

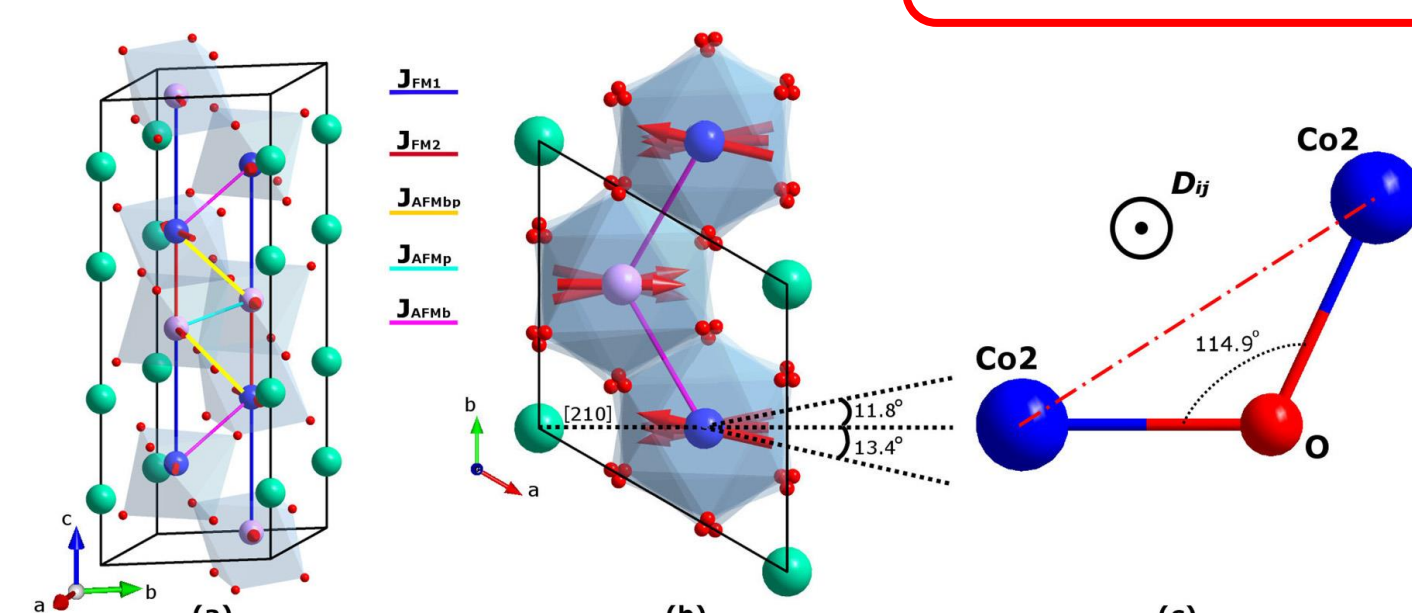
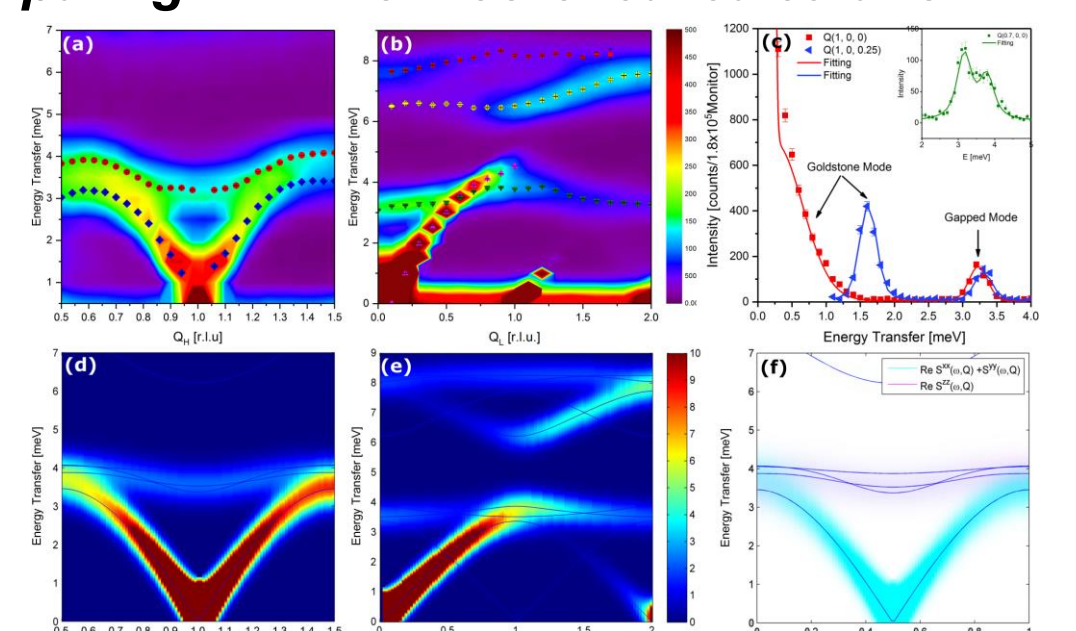


Fig. 9 (a) Crystal structure of  $Co_4Nb_2O_9$  and the exchange paths; (b) magnetic structure and the Dzyaloshinskii-Moriya (DM) interaction.<sup>[2]</sup>

Fig. 10 Inelastic neutron scattering from the spin wave in  $Co_4Nb_2O_9$  measured on Taipan, and Sika, comparing with the theoretical calculation<sup>[2]</sup>



Magnetoelectric material  $Co_4Nb_2O_9$  demonstrates a unique in-plane noncollinear magnetic structure and very special spin dynamics with a large in-plane anisotropy. It was found that the large in-plane anisotropy and DM interaction is the main reason for the large ME coupling in this magnet. This is a collaborative work with Prof. SX Cao in Shanghai Univ.

## Reference

- S. Toth and B. Lake, J. Phys. Condens. Matter 16, 166002 (2015).
- Deng et al. Phys. Rev. B.98.184411(2018)

## Acknowledgement:

We acknowledge the support of the technical and sample environment teams of ACNS.

\*E-mails: gc.deng.ansto@gmail.com